

Strongly-correlated bosons on a dynamical lattice

Daniel González-Cuadra,¹ Przemysław R. Grzybowski,^{1,2} Alexandre Dauphin¹ and Maciej Lewenstein^{1,3}

¹*ICFO-Institut de Ciències Fotòniques, The Barcelona Institute of Science and Technology, Av. Carl Friedrich Gauss 3, 08860 Barcelona, Spain*

²*Faculty of Physics, Adam Mickiewicz University, Umultowska 85, 61-614 Poznań, Poland and*

³*ICREA-Institució Catalana de Recerca i Estudis Avançats, Lluís Companys 23, 08010 Barcelona, Spain*

We study a one-dimensional system of strongly-correlated bosons interacting with a dynamical lattice. A minimal model describing the latter is provided by extending the standard Bose-Hubbard Hamiltonian to include extra degrees of freedom on the bonds of the lattice. We show that this model is capable of reproducing phenomena similar to those present in usual fermion-phonon models. In particular, we discover a bosonic analog of the Peierls transition, where the translational symmetry of the underlying lattice is spontaneously broken. The latter provides a dynamical mechanism to obtain a topological insulator in the presence of interactions, analogous to the Su-Schrieffer-Heeger (SSH) model for electrons. We numerically characterize the phase diagram of the model, which includes different types of bond order waves and topological solitons. Finally, we study the possibility of implementing the model experimentally using atomic systems.

Introduction – The study of interactions between particles and lattice degrees of freedom is of central importance in quantum many-body physics. The interplay between electrons and phonons has been extensively studied, leading to the description of paradigmatic effects such as superconductivity, polaron formation or charge density waves [1, 2]. The analogous problem for bosons, on the other hand, has not been extensively investigated. In one dimension, a system of itinerant particles on a deformable lattice can undergo a Peierls transition [3], characterized by the spontaneous breaking of the lattice translational symmetry. In the fermionic case, the statistical correlations brought about by Pauli’s exclusion principle are sufficient to drive this type of many-body effect, associated with a gap opening around the Fermi surface. In the bosonic case the Fermi surface is lost. However, similar effects still appear in the presence of sufficiently strong interactions, as we report in this work.

The study of boson-lattice problems becomes very relevant in the context of the substantial progress achieved with quantum simulation techniques using atomic systems. Quantum simulators are very versatile platforms where model Hamiltonians can be engineered with an unprecedented degree of control [4, 5]. Ultracold atoms in optical lattices, in particular, allow us to experimentally address systems of strongly-correlated bosons and to study their properties in a controllable environment [6–9]. This was first shown in a seminal experiment for the Bose-Hubbard model [10], leading to the observation of a phase transition between a Mott insulator and a superfluid phase [11]. Since then, larger families of models have been studied—including, for example, different types of interactions [12, 13] or artificial gauge fields [14, 15]. These models provide an interesting platform to study novel and relevant strongly-correlated phenomena, such as supersolid phases [16] or topological order [17].

The simulation of these models rely on the implementation of static optical lattices. The particles do not in-

fluence the lattice structure and, therefore, phonons are usually not taken into account. Trapped ion systems can also be used to simulate many-body Hamiltonians [18–20]. In these systems, phonons appear naturally due to the vibration of the ions inside the trap [21]. These phonons can be used to mediate interactions between different ions and to simulate spin models [22]. However, as opposed to ultracold neutral atoms, trapped ions are confined at the lattice sites, making the simulation of itinerant particles more challenging. Recently, advances in designing systems formed by both neutral atoms and ions [23–30] suggest the possibility of simulating itinerant particles and lattice degrees of freedom simultaneously. This approach was explored for a chain of fermionic atoms, where a Peierls transition was predicted [24].

In this letter, we propose and analyze a one-dimensional model of interacting bosons whose tunneling term is coupled to additional degrees of freedom. The latter provides a minimal model to describe a dynamical lattice. We also discuss a possible experimental scheme with ultracold neutral atoms and trapped ions. The most important result of this work is the discovery of bosonic analogs of Peierls transitions, leading to commensurate and incommensurate Bond Order Waves (BOW). For density $\rho = 1/2$, the latter corresponds to a dynamically generated topological insulator, supporting edge states and topological solitons, similar to the fermionic SSH model [31]. The proposed model provides, therefore, a unique playground to study the interplay between strong boson interactions, lattice dynamics, spontaneous symmetry breaking and topological effects.

Model – We propose a minimal model of strongly correlated bosons interacting with lattice degrees of freedom, by describing the latter with a set of independent

two-level systems. The Hamiltonian reads

$$\hat{H} = -t \sum_i \left(\hat{b}_i^\dagger \hat{b}_{i+1} + \text{h.c.} \right) + \frac{U}{2} \sum_i \hat{n}_i (\hat{n}_i - 1) - \mu \sum_i \hat{n}_i - \alpha \sum_i \left(\hat{b}_i^\dagger \hat{\sigma}_i^z \hat{b}_{i+1} + \text{h.c.} \right) + \frac{\Delta}{2} \sum_i \hat{\sigma}_i^z + \beta \sum_i \hat{\sigma}_i^x, \quad (1)$$

where \hat{b}_i^\dagger creates a boson on the site i and $\hat{n}_i = \hat{b}_i^\dagger \hat{b}_i$ is the number operator. $\hat{\sigma}_i^z$ and $\hat{\sigma}_i^x$ are Pauli operators associated with a spin-1/2 system living on the bond between sites i and $i+1$. The first three terms of (1) correspond to the standard Bose-Hubbard model in the grand canonical ensemble. The next term describes a lattice-dependent boson tunneling. The total hopping through a bond is maximized (resp. minimized) for a spin in the “up” (“down”) state. Finally, the last two terms introduce the spin dynamics. The Hamiltonian (1) bears similarities with other models where spins located on the bonds mediate the interactions between particles, such as quantum link models [32].

In this work, we focus on the regime of quasi-adiabatic spins, i.e., $\beta \ll t$. In this limit, the ground state of the spins depends on the competition between two terms: the energy difference between the spin states in the z axis and the interaction term with the bosons. If one of the two dominates, the expectation value $\langle \hat{\sigma}_i^z \rangle$ will be uniform and close to -1 ($\Delta \gg \alpha$) or $+1$ ($\Delta \ll \alpha$). When the two competing terms are comparable, phases with broken translational symmetry may arise.

Hardcore Bosons – Consider first a completely adiabatic lattice, $\beta = 0$, in the hardcore boson limit, $U \rightarrow \infty$. After a Jordan-Wigner transformation, the model is mapped to a system of spinless fermions in a classical background, given by the spin configuration. It can be shown that, at half filling, the configuration minimizing energy is staggered (Neel order) for values of Δ between two critical points, $\Delta_c^\pm = \frac{4t}{\pi} [\delta \pm (E(1 - \delta^2) - 1)]$, where $\delta = \alpha/t$ and $E(x)$ is a complete elliptic integral of the second kind [33]. From the fermions’ point of view, this leads to the development of a staggered order on the bonds. In this situation, a gap opens at the Fermi surface, and the system becomes insulating. This kind of gap appears when the lattice deformation, which breaks translational invariance, has a wavelength equal to the inverse of the Fermi wavevector k_F . This is the mechanism behind the Peierls instability. Thus, our minimal model is capable of describing analogous phenomena such as those appearing in more complicated fermion-lattice systems, such as the SSH model [31].

Finite Interactions – For finite values of U , the mapping to non-interacting fermions is not possible. We then enter into the strongly-correlated boson regime. To calculate the ground state of the system, we use an MPS-based DMRG algorithm with bond dimension $D = 40$ [34]. We consider a system size of $L = 60$ sites (and

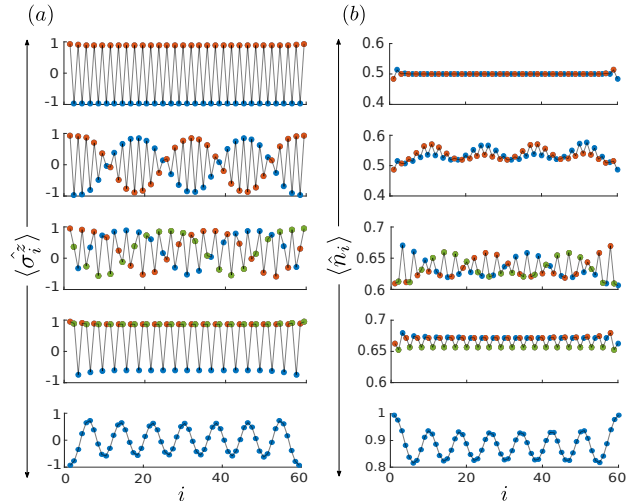


FIG. 1. The spatial structure of bond (a) and site (b) expectation values for $\Delta = 0.85$ and different bosonic densities, showing some of the representative orders that can develop. From above to below: $\rho = 1/2$, $\rho = 1/2 + 2/60$, $\rho = 2/3 - 2/60$, $\rho = 2/3$ and $\rho = 0.88$. Different colors represent different sublattice elements, making explicit the long-wavelength modulations on top of the staggerization.

$L - 1$ bonds), and work with open boundary conditions. We also truncate the maximum number of bosons per site to $n_0 = 2$. This approximation is justified for low densities and strong interactions. In the following calculations, we fix the values of the parameters to $t = 1$, $\alpha = 0.5$ and $\beta = 0.02$ (quasi-adiabatic lattice).

At density $\rho = 1/2$, the Neel order survives in the quantum spin sublattice for finite values of U , and disappears for small interactions. Strong correlations are needed, therefore, to have a bosonic Peierls phase. In Ref. [35], the Bose-Hubbard model on a fixed bond-dimerized lattice was studied, revealing an insulating phase at $\rho = 1/2$, and the presence of topological edge states. Here, the same superlattice structure is obtained in a dynamical way, in the spirit of the original SSH model for fermions and phonons [31]. Although we also observe edge states, a full description of them will be given in a separate work [36]. We focus here on a different topological effect that is also present in the SSH model: the solitonic solutions. These are a consequence of the double degenerate ground state, corresponding to the two inverted staggered patterns, and only occur when quantum fluctuations on the lattice are present.

In the following, we choose $U = 10$, and study the phase diagram of the model in terms of Δ for different bosonic densities ρ . The latter is adjusted by fixing the chemical potential μ . For $\Delta \gg \alpha$ or $\Delta \ll \alpha$, the spin configuration in the ground state is uniform. The boson part of the Hamiltonian (1) is qualitatively similar to the standard Bose-Hubbard model [10], with a Mott insula-

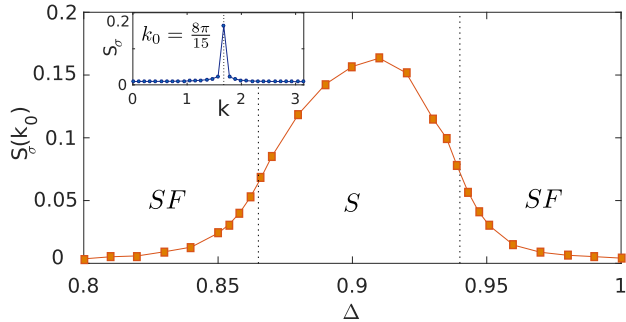


FIG. 2. Inset: Structure factor $S(k)$ for a point in the solitonic phase (S), for $\rho = 0.733$ and $\Delta = 0.90$. A clear peak is observed at $k_0 = 8\pi/15$. In the figure, the structure factor at k_0 is shown in terms of Δ , qualitatively distinguishing between this phase and the uniform SF one. The exact location of the critical points (dotted lines) is found by performing a finite-size scaling of the fidelity susceptibility [33]

tor (MI) and a superfluid phase (SF). In an intermediate regime ($\Delta \approx 0.6-1.0$), the translational symmetry is broken in the ground state for a substantial range of bosonic densities. In Fig. 1, we show the spatial structure on the bonds (a) and sites (b) for $\Delta = 0.85$. For $\rho = 1/2$ and $2/3$, the new unit cell is enlarged to two and three sites, respectively. Boson density variations (b) are small or absent in those cases. For different values of Δ , a similar pattern occurs for $\rho = 1/3$ (not shown), where the unit cell is composed of one “up” and two “down” spins. For densities close to the mentioned ones, long wavelength modulations appear on top of the corresponding patterns. These correspond to *solitonic* solutions where the underlying order—staggered in the half-filled case—is reversed periodically forming kinks; the “extra” bosons or holes lead to increased density modulations, located around the kinks (2nd or 3rd row in panel (b)), in analogy with the fermionic SSH [31]. Finally, close to $\rho = 1$, long wavelength structures also appear. We find that the bosonic hopping $\langle \hat{b}_i^\dagger \hat{b}_{i+1} + \text{h.c.} \rangle$ values present the same spatial pattern as $\hat{\sigma}_i^z$ in all the cases. In the following, we will focus only on the latter quantity for simplicity. The ground states shown in Fig. 1 possess long-range bond order. We will refer to the corresponding quantum phases as *Bond Order Waves* (BOW). In many cases, the bond order is accompanied by density waves (Fig. 1).

We consider the spin structure factor

$$S_\sigma(k) = \frac{1}{L} \sum_{i,j} e^{(x_i - x_j)ki} \langle (\hat{\sigma}_i^z - \bar{\sigma}^z) (\hat{\sigma}_j^z - \bar{\sigma}^z) \rangle, \quad (2)$$

with $\bar{\sigma}^z = \sum_i \langle \hat{\sigma}_i^z \rangle / L$. This quantity develops a peak for some k_0 in the presence of long-range order, and its height can be used as an order parameter. Fig. 2 shows S_σ^{\max} in terms of Δ for $\rho = 0.733$, which qualitatively distinguishes a uniform SF phases from a solitonic BOW. The

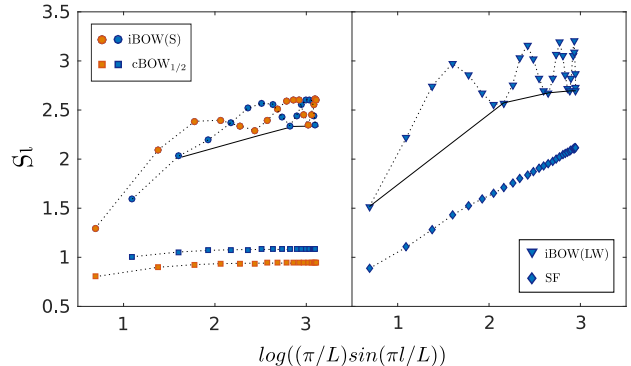


FIG. 3. Entanglement entropy S_l , including finite size corrections [37], in terms of the block size l . We show the scaling behavior for different phases, the latter being linear only in the SF case, signaling that this phase is gapless. For the gapped phases the entropy saturates. The spatial inhomogeneities in the ground state influence the scaling. A meaningful analysis of the scaling is done by increasing the size of the block l by the system’s unit cell size. This is depicted by a solid black line for the iBOW phases. In the left panel, odd and even values are represented in different colors.

inset of the figure shows S_σ for $\Delta = 0.90$, where a peak develops for $k_0 = 8\pi/15$. From this wavevector, an order wavelength can be defined as $\lambda_0 = 2\pi/k_0$. We note that, in this case, λ_0 is not an integer factor of the lattice spacing a (fixed to one here). This is also the case for the other solitonic and long-wavelength BOW phases. We refer to these orders as *incommensurate* (iBOW). For $\rho = 1/3, 1/2$ and $2/3$, however, S_σ presents a peak at $\pi/3, \pi$ and $2\pi/3$, respectively, and their corresponding wavelengths are of the form aN . We call the latter *commensurate* orders (cBOW).

All the BOW phases we observe are gapped. This can be seen by calculating the scaling of the entanglement entropy between a block of size l and the rest of the system, $S_l = -\text{Tr}(\rho_l \log \rho_l)$, where $\rho_l = \text{Tr}_{L-l} |\Psi\rangle\langle\Psi|$ is the reduced density matrix corresponding to the block. In one-dimensional systems, gapped phases follow an area law [38], and S_l saturates when increasing l . For gapless phases, however, it grows logarithmically in the block’s size [37]. Fig. 3 shows the scaling of the entanglement entropy and indicates that only the SF phase is gapless. The solitonic phases present in our model are qualitatively different, therefore, from those appearing in the extended Bose-Hubbard model [39], which are gapless.

Interestingly, some of these gapped phases are compressible, with compressibility $\kappa = \frac{\partial \rho}{\partial \mu} \neq 0$. This is in contrast to the behavior of many phases in bosonic models, where the presence of a gap usually implies incompressibility. The latter is commonly used as a way of detecting superfluidity in one-dimensional systems, due to the lack of an order parameter—as a consequence of the Mermin-Wagner-Hohenberg theorem [40–42]. Fig. 4

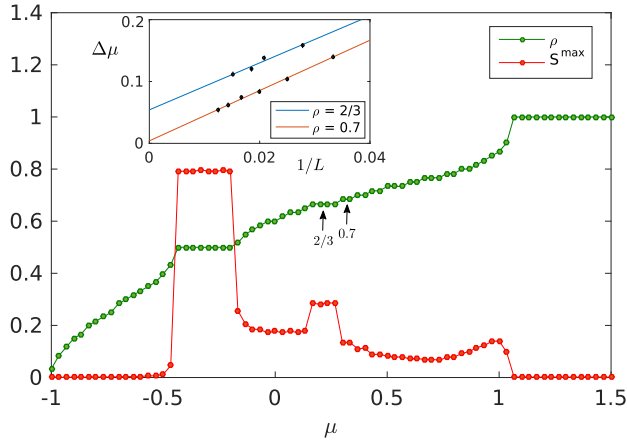


FIG. 4. In the figure, we show the density ρ and maximum structure factor S^{\max} in terms of the chemical potential μ for $\Delta = 0.87$ and $L = 60$. The structure factor has non-zero values for the BOW phases. Plateaus in the density are related to incompressible phases, but they can also appear as finite size effects. In the inset, we show the size of the plateau $\Delta\mu$ for different system sizes for a cBOW phase ($\rho = 2/3$) and a solitonic iBOW one ($\rho = 0.7$), and the extrapolation to the thermodynamic limit. Compressibility κ and structure factor are sufficient to distinguish between the observed phases.

depicts the density ρ in terms of μ for $\Delta = 0.87$. Here, a superfluid phase occurs for $0 < \rho < 1/2$, and BOW phases appear for $1/2 \leq \rho < 1$. Finally, $\rho = 1$ corresponds to a Mott insulator. The plateaus in the $\mu - \rho$ line signal the incompressible phases, which, in this case, correspond to a cBOW phase at $\rho = 1/2$ and $\rho = 2/3$. The finite size scaling of other plateaus (inset) reveals that the iBOW phases are indeed compressible.

In the hardcore limit, the presence of a gap and a non-zero compressibility can be understood using the single-particle fermionic picture. When the density of particles increases, the wavevector k_0 , equal to k_F , changes continuously. The extra particles accommodate below the gap, which is displaced and does not vanish. For strongly-correlated bosons the mechanism is more complicated, although some of the properties are equivalent to the fermionic case. In particular, we see that the order wavevector k_0 changes continuously with the bosonic density ρ . The presence of incompressible cBOW phases, however, implies that orders with commensurate wavelengths are more stable under small but finite changes of the chemical potential. Fig. 4 shows the maximum value of the structure factor (S^{\max}) as a function of μ . It is zero for the uniform phases (Mott insulator and superfluid) and it changes continuously among the BOW phases, except for the commensurate orders where it clearly stands out. Since S^{\max} represents an order parameter, this behavior corresponds to finite changes in the free energy as the density is varied, meaning that these *pinned* wavelengths are energetically more stable. This is the under-

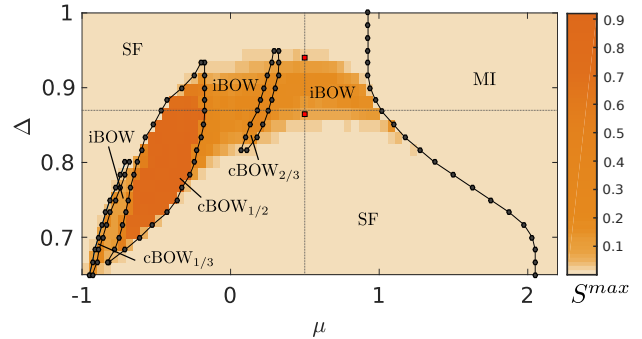


FIG. 5. Phase diagram of the Hamiltonian (1) for a system size of $L = 60$ in terms of the parameter Δ and the chemical potential μ . The solid black lines delimit the incompressible phases: the different cBOW and the MI. In the background, the maximum value of the structure factor is represented in different colors, qualitatively distinguishing between the iBOW and SF phases. The dotted lines correspond to the cases with constant $\mu = 0.5$ and $\Delta = 0.87$, shown in Fig. 2 and 3, respectively. For the former, the red squares mark two critical points in the thermodynamic limit.

lying mechanism that explains the zero compressibility of the cBOW phases.

For a wide range of values of Δ we calculate both the plateau size and the maximum structure factor in terms of μ . These two properties are sufficient to identify all the phases of the model. The results are summarized in the phase diagram shown in Fig. 5. Inside the Mott insulator phase, the spins are uniform and $\hat{\sigma}_i^z$ changes continuously from $+1$ to -1 as Δ increases. As a consequence, the boundary between this phase and the superfluid is modified, the former being enlarged. The phase diagram also provides information about the extension of the BOW phases. In particular, we observed that, for this choice of parameters, cBOW $_{1/2}$ is more stable than cBOW $_{2/3}$ and cBOW $_{1/3}$.

Experimental implementation – To realize the boson-spin Hamiltonian (1), we consider first a gas of ultracold bosonic atoms in an optical lattice, described by the standard Bose-Hubbard Hamiltonian. A second optical lattice, trapping either neutral or charge atoms, is introduced, placing its minima between two minima of the first lattice. The atoms corresponding to the second lattice have two internal degrees of freedom—representing the spin degrees of freedom—and the potential is deep enough to confine them at each minima. As shown in [23, 25, 43, 44], in this situation, the hopping of the moving particles between two neighboring sites is influenced by the internal state of the corresponding spin, giving rise to the desired spin-boson interaction. The on-site boson interaction term can be influenced by the internal state of the spins. However, this dependence is very weak [25], and we neglect it here. The spin part of the Hamiltonian can be implemented as follows: the energy difference

between the two spin states is obtained by introducing an external magnetic field, and the spin flipping is enforced using laser-assisted transitions between the two states. This strategy is valid both when the impurity corresponds to a neutral atom or to an ion. Although the value of the coupling α in the boson-spin interaction might be difficult to tune in an experiment, the phases we show in this work are present for a broad range of values of this parameter. One could, in principle, drive the system to a non-trivial phase by changing the energy difference Δ between the two spin states. The different phases could then be detected by measuring the spin structure factor [45–47] and the compressibility in the atomic system [48, 49].

Summary – We introduced a boson-spin Hamiltonian that models the behavior of strongly-correlated bosons on a dynamical lattice, and demonstrated the possibility of obtaining bosonic analogs of the Peierls phase. We characterized the phases of the system in the quasi-adiabatic limit (slow lattice dynamics), using the spin structure factor, entanglement entropy scaling and compressibility. We found, besides the uniform SF and MI phases, compressible and incompressible Bond Order Waves. We also discuss the possibility of implementing the model using ultracold atoms and ions trapped in optical lattices. In the future, it would be interesting to study more extensively the topological properties of the model, as well as the regime of non-adiabatic spins.

The authors thank A. Celi, E. Tirrito, A. Piga, L. Tarruell and R. W. Chhajlany for useful discussions. This work has been supported by Spanish MINECO (Severo Ochoa SEV-2015-0522 and FisicaTeAMO FIS2016-79508-P), the Generalitat de Catalunya (SGR 874 and CERCA), Fundacio Privada Cellex, and EU grants OSYRIS (ERC-2013-AdG Grant 339106), QUIC (H2020-FETProAct-2014 641122). D. González-Cuadra is financed by the ICFOstepstone Programme of the European Commission (COFUND-DP, H2020-MSCA-COFUND-2014, GA n 665884). A. Dauphin is financed by a Cellex-ICFO-MPQ fellowship.

-
- [1] A. Altland and B. Simons, *Condensed Matter Field Theory* (Cambridge University Press, 2006).
- [2] D. Emin, *Polarons* (Cambridge University Press, 2012).
- [3] R. Peierls, *Quantum Theory of Solids*, International series of monographs on physics (Clarendon Press, 1955).
- [4] I. Buluta and F. Nori, *Science* **326**, 108 (2009).
- [5] J. I. Cirac and P. Zoller, *Nat. Phys.* **8**, 264 (2012).
- [6] D. Jaksch and P. Zoller, *Annals of Physics* **315**, 52 (2005).
- [7] I. Bloch, J. Dalibard, and W. Zwerger, *Rev. Mod. Phys.* **80**, 885 (2008).
- [8] I. Bloch, *Nat. Phys.* **1**, 23 (2005).
- [9] M. Lewenstein, A. Sanpera, and V. Ahufinger, *Ultracold Atoms in Optical Lattices: Simulating Quantum Many-body Systems* (Oxford University Press, Oxford, 2017).
- [10] M. P. A. Fisher, P. B. Weichman, G. Grinstein, and D. S. Fisher, *Phys. Rev. B* **40**, 546 (1989).
- [11] M. Greiner, O. Mandel, T. Esslinger, T. W. Hänsch, and I. Bloch, *Nature* **415**, 39 (2002).
- [12] V. W. Scarola and S. Das Sarma, *Phys. Rev. Lett.* **95**, 033003 (2005).
- [13] O. Dutta, M. Gajda, P. Hauke, M. Lewenstein, D.-S. Lühmann, B. A. Malomed, T. Sowiński, and J. Zakrzewski, *Rep. Prog. Phys.* **78**, 066001 (2015).
- [14] N. Goldman, G. Juzelinias, P. Öhberg, and I. B. Spielman, *Rep. Prog. Phys.* **77**, 126401 (2014).
- [15] J. Dalibard, F. Gerbier, G. Juzeliūnas, and P. Öhberg, *Rev. Mod. Phys.* **83**, 1523 (2011).
- [16] G. G. Batrouni, F. Hébert, and R. T. Scalettar, *Phys. Rev. Lett.* **97**, 087209 (2006).
- [17] E. G. Dalla Torre, E. Berg, and E. Altman, *Phys. Rev. Lett.* **97**, 260401 (2006).
- [18] R. Blatt and C. F. Roos, *Nat. Phys.* **8**, 277 (2012).
- [19] C. Schneider, D. Porras, and T. Schätz, *Rep. Prog. Phys.* **75**, 024401 (2012).
- [20] M. Johanning, A. F. Varn, and C. Wunderlich, *J. Phys. B: At. Mol. Opt. Phys.* **42**, 154009 (2009).
- [21] D. Leibfried, R. Blatt, C. Monroe, and D. Wineland, *Rev. Mod. Phys.* **75**, 281 (2003).
- [22] D. Porras and J. I. Cirac, *Phys. Rev. Lett.* **92**, 207901 (2004).
- [23] A. Negretti, R. Gerritsma, Z. Idziaszek, F. Schmidt-Kaler, and T. Calarco, *Phys. Rev. B* **90**, 155426 (2014).
- [24] U. Bissbort, D. Cocks, A. Negretti, Z. Idziaszek, T. Calarco, F. Schmidt-Kaler, W. Hofstetter, and R. Gerritsma, *Phys. Rev. Lett.* **111**, 080501 (2013).
- [25] R. Gerritsma, A. Negretti, H. Doerk, Z. Idziaszek, T. Calarco, and F. Schmidt-Kaler, *Phys. Rev. Lett.* **109**, 080402 (2012).
- [26] J. Joger, A. Negretti, and R. Gerritsma, *Phys. Rev. A* **89**, 063621 (2014).
- [27] A. Härter and J. H. Denschlag, *Contemporary Physics* **55**, 33 (2014).
- [28] A. T. Grier, M. Cetina, F. Oručević, and V. Vuletić, *Phys. Rev. Lett.* **102**, 223201 (2009).
- [29] C. Zipkes, S. Palzer, C. Sias, and M. Köhl, *Nature* **464**, 388 (2010).
- [30] S. Schmid, A. Härter, and J. H. Denschlag, *Phys. Rev. Lett.* **105**, 133202 (2010).
- [31] A. J. Heeger, S. Kivelson, J. R. Schrieffer, and W. P. Su, *Rev. Mod. Phys.* **60**, 781 (1988).
- [32] U.-J. Wiese, *Annalen der Physik* **525**, 777 (2013).
- [33] See Supplementary Material for further details on the ground state properties of the model in the hardcore limit, the fidelity susceptibility and the calculation of the critical points Δ_c between the superfluid and supersolid phases.
- [34] U. Schollwöck, *Annals of Physics* **326**, 96 (2011).
- [35] F. Grusdt, M. Höning, and M. Fleischhauer, *Phys. Rev. Lett.* **110**, 260405 (2013).
- [36] D. González-Cuadra, P. R. Grzybowski, A. Dauphin, and M. Lewenstein, (unpublished).
- [37] P. Calabrese and J. Cardy, *J. Stat. Mech. Theory Exp.* **2004**, P06002 (2004).
- [38] J. Eisert, M. Cramer, and M. B. Plenio, *Rev. Mod. Phys.* **82**, 277 (2010).

- [39] T. Mishra, R. V. Pai, S. Ramanan, M. S. Luthra, and B. P. Das, *Phys. Rev. A* **80**, 043614 (2009).
- [40] N. D. Mermin and H. Wagner, *Phys. Rev. Lett.* **17**, 1133 (1966).
- [41] P. C. Hohenberg, *Phys. Rev.* **158**, 383 (1967).
- [42] S. Coleman, *Commun. Math. Phys.* **31**, 259 (1973).
- [43] A. Micheli, A. J. Daley, D. Jaksch, and P. Zoller, *Phys. Rev. Lett.* **93**, 140408 (2004).
- [44] J. M. Schurer, R. Gerritsma, P. Schmelcher, and A. Negretti, *Phys. Rev. A* **93**, 063602 (2016).
- [45] R. A. Hart, P. M. Duarte, T.-L. Yang, X. Liu, T. Paiva, E. Khatami, R. T. Scalettar, N. Trivedi, D. A. Huse, and R. G. Hulet, *Nature* **519**, 211 (2015).
- [46] M. F. Parsons, A. Mazurenko, C. S. Chiu, G. Ji, D. Greif, and M. Greiner, *Science* **353**, 1253 (2016).
- [47] A. Mazurenko, C. S. Chiu, G. Ji, M. F. Parsons, M. Kanász-Nagy, R. Schmidt, F. Grusdt, E. Demler, D. Greif, and M. Greiner, *Nature* **545**, 462 (2017).
- [48] U. Schneider, L. Hackermüller, S. Will, T. Best, I. Bloch, T. A. Costi, R. W. Helmes, D. Rasch, and A. Rosch, *Science* **322**, 1520 (2008).
- [49] V. W. Scarola, L. Pollet, J. Oitmaa, and M. Troyer, *Phys. Rev. Lett.* **102**, 135302 (2009).

Supplementary Material to “Strongly-correlated bosons on a dynamical lattice”

Daniel González-Cuadra,¹ Przemysław R. Grzybowski,^{1,2} Alexandre Dauphin¹ and Maciej Lewenstein^{1,3}

¹*ICFO-Institut de Ciències Fotòniques, The Barcelona Institute of Science and Technology, Av. Carl Friedrich Gauss 3, 08860 Barcelona, Spain*

²*Faculty of Physics, Adam Mickiewicz University, Umultowska 85, 61-614 Poznań, Poland and*

³*ICREA-Institució Catalana de Recerca i Estudis Avançats, Lluís Companys 23, 08010 Barcelona, Spain*

In this Supplementary Material we discuss additional details concerning the hardcore limit of the boson-spin Hamiltonian (1) introduced in the main text, and the calculation of the superfluid-soliton phase transition using the fidelity susceptibility.

HARDCORE BOSONS IN A STATIC LATTICE

Consider the boson-spin Hamiltonian (1) of the main text for a static lattice, with $\beta = 0$. In the hardcore boson limit, $U \rightarrow \infty$, a Jordan-Wigner transformation maps the system to a model of spinless fermions. The transformed Hamiltonian is quadratic in the fermionic operators,

$$\hat{H} = -t \sum_i \left(\hat{c}_i^\dagger \hat{c}_{i+1} + \text{h.c.} \right) - \mu \sum_i \hat{n}_i - \alpha \sum_i \left(\hat{c}_i^\dagger \hat{\sigma}_i^z \hat{c}_{i+1} + \text{h.c.} \right) + \frac{\Delta}{2} \sum_i \hat{\sigma}_i^z, \quad (1)$$

where \hat{c}_i^\dagger and \hat{c}_i are creation and annihilation fermionic operators, respectively, and $\hat{n}_i = \hat{c}_i^\dagger \hat{c}_i$ is the number of fermions at site i . This Hamiltonian (1) describe a system of non-interacting fermions coupled to classical degrees of freedom. For a given configuration of the classical variables, the Hamiltonian can be diagonalized analytically using a single-particle picture.

For large enough values of Δ the fermionic and spin subsystems decouple. The spin configuration that minimizes the total energy is the one with all spins down. Conversely, for $\Delta = 0$ the spin configuration in the ground state of the system is the one that minimizes the energy of the fermion subsystem. For $\rho \notin \{0, 1\}$, this happens when all spins are in the up state, making the fermion hopping uniform and maximal. For other values of Δ , the energies of these two configurations become comparable and other spin configurations are possible in the ground state.

We focus on the half-filling case ($\rho = 1/2$). In the uniform “down” and “up” spin configurations, the ground state energy per site is $\varepsilon = -\Delta/2 - 2(t - \alpha)/\pi$ and $\varepsilon = \Delta/2 - 2(t + \alpha)/\pi$, respectively. There is another important spin configuration, the Neel ordered or staggered spin structure. In this configuration, the values of the fermion hopping are also staggered ($t \pm \alpha$), the unit cell doubles and a gap opens around the Fermi energy. There are two branches of single-particle energies in the reduced Brillouin zone ($-\pi/2 < k < \pi/2$),

$$\varepsilon_{\pm}(k) = \pm 2t \sqrt{\delta^2 \sin^2 k + \cos^2 k}, \quad (2)$$

where $\delta = \alpha/t$. This leads to a ground state energy per site of $\varepsilon = -2tE(1 - \delta^2)/\pi$ where $E(x)$ is complete elliptic integral of the second kind. By comparing the aforementioned energies, we conclude that the staggered spin pattern energy is lower between two critical values of the parameter Δ ,

$$\Delta_c^{\pm} = \frac{4t}{\pi} [\delta \pm (E(1 - \delta^2) - 1)]. \quad (3)$$

On the other hand, the uniform “down” and uniform “up” configurations have a lower energy for $\Delta > \Delta_c^+$ and $\Delta < \Delta_c^-$, respectively. We have checked numerically that, indeed, these configurations correspond to the ground state of the system in the respective regimes, being the only possible ones at half filling.

SOLITON - SUPERFLUID PHASE TRANSITION

The Bond Order Wave phases can be easily characterized by means of the compressibility, allowing us to locate the transitions between these phases and the soliton and superfluid ones for finite system sizes. Distinguishing between these two, however, is more complicated, since both of them are compressible. The solitonic and superfluid phases can still be qualitatively distinguished using the structure factor as an order parameter, since the translational invariance symmetry is spontaneously broken in the solitonic phase. However, the exact location of the corresponding critical points is challenging for finite sizes. For this reason, we use the fidelity susceptibility χ_{FS} [1] to find the critical points in the thermodynamic limit. This quantity can be calculated using the following expression,

$$\chi_{FS}(\Delta) = \lim_{\delta \rightarrow 0} \frac{-2 \log |\langle \Psi_0(\Delta) | \Psi_0(\Delta + \delta) \rangle|}{\delta^2} \quad (4)$$

The fidelity susceptibility χ_{FS} shows a clear peak near a quantum phase transition, even for small systems. Figure 1 shows χ_{FS} in terms of Δ for different system sizes and a fixed density of $\rho = 0.733$, corresponding to a vertical cut in the phase diagram of the system (Fig. 5 in the main text). The critical points are found at $\Delta_1 = 0.865$ and $\Delta_2 = 0.940$, by extrapolating the position of the peaks

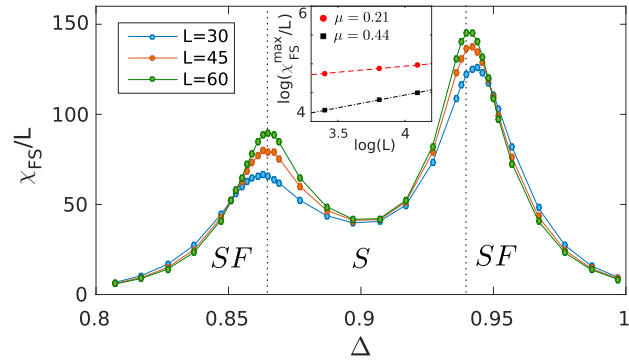


FIG. 1. The exact location of the critical points (dotted lines) between the SF and S phases is found using the fidelity susceptibility χ_{FS} . In the figure, χ_{FS} is represented in terms of Δ for different system sizes. The critical points are located by extrapolating the positions of the peaks, where χ_{FS} grows algebraically with the system size, $\chi_{FS}/L \sim L^\mu$. In the inset, the scaling of the value of χ_{FS} at the peak is represented for the left (black) and right (red) ones. The critical coefficients μ are obtained by fitting it to a line.

in the thermodynamic limit. In those points, the value of χ_{FS} grows algebraically as $\chi_{FS}/L \sim L^\mu$ (inset). The critical exponents are different in the two transitions.

[1] S.-J. Gu, *International Journal of Modern Physics B* **24**, 4371 (2010).